Prod. Eng. Res. Devel. (2017) 11:435–444
DOI 10.1007/s11740-017-0761-4

PRODUCTION PROCESS

Micro milling of titanium alloy Ti-6Al-4V: 3-D finite element modeling for prediction of chip flow and burr formation

Tuğrul Özel[1] · **Alaa Olleak**[1] · **Thanongsak Thepsonthi**[2]

Received: 21 March 2017 / Accepted: 7 August 2017 / Published online: 14 August 2017

Abstract Cutting process of titanium alloy Ti-6Al-4V is considered difficult due to chemical affinity between tool and work material, adhesion, built-up edge and burr formation, and tool wear resulting in loss of productivity. Three dimensional (3-D) chip flow together with local field variables such as temperature, elastic/plastic strain, strain-rate and velocity in the shear zones during micro milling process can be predicted using continuum-mechanics based 3-D Finite Element (FE) modelling and simulation of elastic/viscoplastic work material deformations. This paper provides much needed process insight for chip flow, built-up edge and burr formation by using modeling work with experimental validation. Scanning electron microscopic (SEM) observation of the 3-D chip morphology and burrs demonstrate ductile fractured surfaces together with localized instability and failure behaviors. FE simulations are utilized to investigate the effects of micro milling operation i.e. up and down milling and tool edge radius on 3-D chip flow, built-up edge, and 3-D burr formation. Simulated results are compared with measurements of chip morphology, shape, and dimensions together with tool edge condition of built-up edge and chip adhesion yielding to good agreements.

Keywords Chip · Milling · Titanium · Finite element method

✉ Tuğrul Özel
ozel@rutgers.edu

[1] Manufacturing and Automation Research Laboratory, Rutgers, The State University of New Jersey Industrial and Systems Engineering, 96 Frelinghuysen Road, Piscataway, NJ 08854, USA

[2] Department of Industrial Engineering, Burapha University, Chonburi, Thailand

1 Introduction

Titanium and its alloys find growing number of applications in aerospace, pharmaceutical, and biomedical device industries due to their high strength-to-weight ratio, corrosion resistance, and biocompatibility [14]. For instance, titanium alloys are used in orthopedics and dentistry as biomaterials for bone-replacing implant applications. Also, titanium implants are compatible with magnetic resonance imaging and computed tomography imaging procedures, so they do not interfere with those procedures if the patient needs them after the implant is made [13]. The increasing demands for such components with micro features in these applications alongside stringent quality regulations resulted in researching mechanical micro machining processes to be utilized for production. Micro cutting and micro milling processes provide distinct advantages including flexibility, higher material removal rates, and lower cost in manufacturing of 3-D parts with high precision [6]. However, micro milling of titanium alloys is challenging mainly due to rapid tool wear associated with the chemical affinity of titanium alloys with cutting tool materials such as tungsten carbide, and its low thermal conductivity [9]. Micro milling of difficult-to-cut materials such as titanium alloys suffers from intense adhesion and built-up edge development, severe burr formation and increased roundness of cutting edge due to rapid tool wear and grain fracture [2].

Typically milling with end mills smaller than Ø = 1 mm in diameter is considered micro milling. Micro milling utilizes end mills both with flat- and ball-bottom as small as Ø = 0.2 mm or less in diameters. As a result, cutting mechanics and dynamics is much different than meso/macro scale milling. Micro milling continues to attract research studies ranging from understanding process mechanics using mechanistic modeling [1] and finite

element modelling (Özel et al. [22]; Thepsonthi and Özel [19]) to investigating process dynamics [15] and associated chatter vibrations [21] among many other studies.

In micro end mills, a typical edge roundness that is equal or less than $r_\beta = 3$ μm can be obtained using various techniques [5]. However, edge roundness of the tool or cutting edge radius (r_β) has a known effect on promoting lower shear angles, more ploughing and formation of top burrs, and higher elastic deformations and elastic recovery of the machined surface on the work material with increased difficulty in material separation, surface waviness, and surface roughness [3, 16, 20]. Increased edge roundness may be due to abrasive wear of the cutting edge geometry and can continuously increase with longer cutting distances.

Burr formation mechanism is very complicated involving plastic and elastic deformations which are influenced by material properties, tool geometry, and machining parameters. There is significant influence of titanium alloy's microstructure on burr dimensions, cutting forces, and built-up edge [7]. Top burrs begin to form during tool rotation at lower undeformed chip thickness regions at the exit locations or down milling sections of the full immersion [4]. On the other hand, chip flow provided with the helix angle of the micro end mill flutes and resultant chip curling due to plastic deformations alongside associated burr formation can be best investigated through finite element simulation of 3-D chip formation process [18].

The purpose of this work and the leitmotif of this paper is obtaining a deeper process insight in micro milling using chip formation simulations with the help of a rich set of physical variables such as plastic chip flow, plastic strain, principle stresses, and temperatures for making predictions in process outputs such as chip shape and dimensions, chip formation angles, burr formation dimensions and angles, shear angles, cutting forces, and built-up edge formation. While use of lubricants and coolants are common methods in machining of titanium alloys, dry machining has importance in achieving high sustainability and minimum ecological footprint. Therefore, dry micro milling of titanium alloy Ti-6Al-4V is the subject of investigations presented in this paper.

In micro-end milling with a flat bottom micro end mill with known rake angle (γ), helix angle (β), and an edge radius (r_β), certain micro end mill rotation angle (ϕ) can be designated as chip formation angle (ϕ_{cfa}) where minimum undeformed chip thickness is achieved and a chip begins to form and a top burr formation angle (ϕ_{bfa}) can be defined where top burr formation initiates and the shear angle (ϕ_s) at the surface along the chip flow direction gradually declines as illustrated in Fig. 1. Therefore, it is possible to establish a chip flow angle (η_c) at the root of the chip with respect to the flat bottom of the tool.

2 Experimental approach

Uncoated two-flute flat-bottom end mills made with ultrafine grain tungsten carbide in a cobalt matrix (WC/Co) from Kyocera company are used in micro milling of titanium alloy Ti-6Al-4V (335 HV in hardness) under dry conditions (no lubricants or coolant applied). Micro end mill tool diameter is about Ø = 0.508 mm with a helix angle of $\beta = 30°$ and has a cutting length of $l_c = 762$ μm. Micro end mills were inspected with SEM and a mean edge radius of $r_\beta = 3 \pm 0.5$ μm was measured. Micro end mills are mounted with $l_t = 15$ mm tool overhand in a precision collet and ceramic-bearing-electrically-driven precision spindle (NSK ASTRO-E 800) and full immersion micro milling of $a_p = 0.1$ mm deep concentric circular slots were machined by using cutting parameters of a surface cutting speed of $v_c = 50$ m/min and a feed rate of $f_z = 4.5$ μm/ tooth. Precision alignment of the micro-end mill with the workpiece was achieved by monitoring with a CCD camera and commanding the three-axis mechanical bearing, ball screw positioning stages (Aerotech ATS100-200, position accuracy of ±1 μm) accordingly.

The chips and the micro-milled workpiece sections were collected from the experiments and investigated using scanning electron microscopy (SEM). The condition of the micro end mill geometry was also monitored after cutting $l_{cut} = 100$ mm distances of as well. A cutting distance of $l_{cut} = 200$ mm resulted in an edge roundness of $r_\beta = 6.4$ μm, and $l_{cut} = 500$ mm resulted in an edge roundness $r_\beta = 12.6$ μm. Therefore, three levels of edge roundness was selected in the FE simulations as $r_\beta = 3$ μm for unworn, $r_\beta = 6$ μm for the slightly worn case after cutting $l_{cut} = 200$ mm, and $r_\beta = 12$ μm for the worn case after cutting of $l_{cut} = 500$ mm distance.

3 Finite element model

3-D finite element modelling of micro milling was done using Finite Element Method (FEM) software DEFORM 3D. The workpiece was considered as viscoplastic material due to the computational cost and tool was considered as a rigid body in the 3-D FEM model. A CAD model of the flat bottom end mill was created by having measured geometrical features as the physical micro-end milling tool. The rake angle at $z = 0$ location of the tool was measured about $\gamma = 15°$. For exploring the effects of tool edge roundness due to increasing tool wear, 3-D CAD models with edge radii of $r_\beta = 3$ μm, $r_\beta = 6$ μm, and $r_\beta = 12$ μm were created for unworn, slightly worn, and worn cases respectively. In 3-D FEM model, the tool was meshed with 3×10^4 elements (between 0.5 and 1.5 μm in size) and only the active cutting

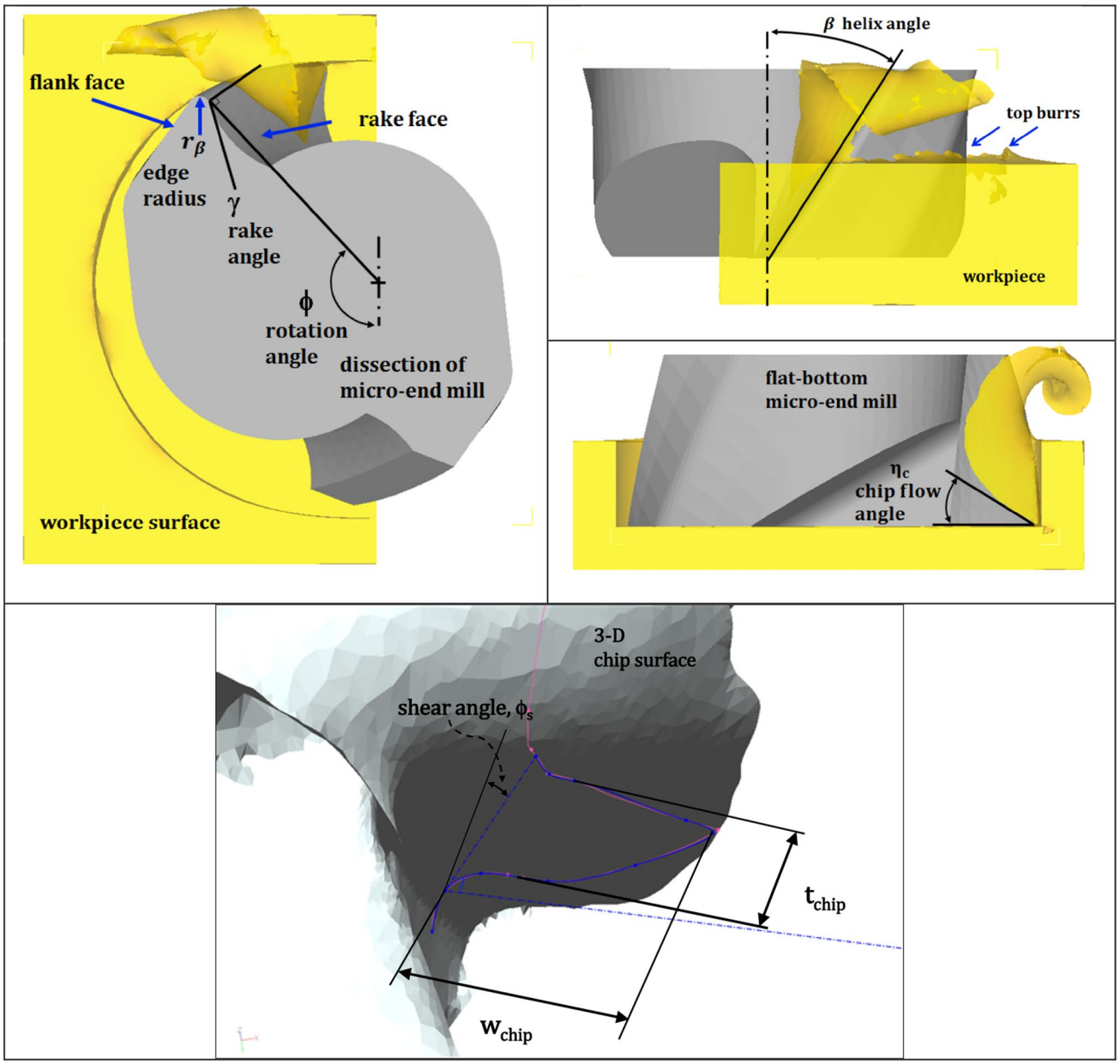

Fig. 1 Full immersion micro-end milling with tool and chip angles

edge was defined with a very fine mesh in order to accurately represent the tool edge geometry.

A material constitutive model with thermal and strain softening at elevated strain and temperatures for the plastic deformations in titanium alloy Ti-6Al-4V was employed.

$$\sigma = \left[A + B\varepsilon^n\left(\frac{1}{exp(\varepsilon^a)}\right)\right]\left[1 + Cln\frac{\dot{\varepsilon}}{\dot{\varepsilon}_0}\right]\left[1 - \left(\frac{T - T_0}{T_m - T_0}\right)^m\right] \times \left[D + (1 - D)\left[\tanh\left(\frac{1}{(\varepsilon + p)^r}\right)\right]^s\right] \quad (1)$$

where $D = 1 - \left(\frac{T}{T_m}\right)^d$, $p = \left(\frac{T}{T_m}\right)^b$, σ is flow stress, ε is true strain, $\dot{\varepsilon}$ is true strain rate, $\dot{\varepsilon}_0$ is reference true strain rate ($\dot{\varepsilon}_0 = 10^{-5}$), T is work temperature, T_m is material melting temperature ($T_m = 1450$ °C), T_0 is ambient temperature ($T_0 = 20$ °C). The modified material model parameters of A, B, n, a, C, m, d, b, r, s are the model constants. A is the yield strength at room temperature, B is the strain dependent strength constant, n is the strain hardening exponent, C is the strain hardening constant, m is thermal softening exponent, a is the strain softening exponent, b, d, r, and s are

Table 1 Temperature-dependent (T in °C) properties of materials

Property	Ti-6Al-4V	WC/Co
E (MPa)	$-0.7412\times T$ (°C) $+1{,}13{,}375$	5.6×10^5
α (mm mm^{-1} °C^{-1})	$3\times10^{-9}\times T$ (°C) $+7.10^{-6}$	4.7×10^{-6}
λ (N s^{-1} °C^{-1})	$7.039\times e^{0.0011\times T\,(°C)}$	55
c_p (N mm^{-2} °C^{-1})	$2.24\times e^{0.0007\times T\,(°C)}$	$0.005\times T$ (°C) $+2.07$

exponents for temperature-dependent flow softening behaviour. The values of $A=782.7$ MPa, $B=498.4$ MPa, $n=0.28$, $a=2$, $C=0.028$, $m=1.0$, $d=0.5$, $r=2$, $b=5$, $s=0.05$ have been utilized in this model [18, 19]. Temperature-dependent properties of work and tool materials used in the 3-D FE model including Young's modulus (E), thermal expansion (α), thermal conductivity (λ), and heat capacity (c_p) are given in Table 1.

The heat generated at the cutting zone was allowed to transfer throughout the micro-end mill and workpiece with a higher than usual heat transfer coefficient of 10^7 kW s^{-1} mm^{-1} °C^{-1} as implemented due to very short contact duration (0.625 ms) during single-tooth-pass in micro milling at cutting conditions considered and to generate sufficient temperature rise for chip formation. Also heat convection to the environment is allowed. Friction at the tool-workpiece contact was modeled considering both sticking and sliding contacts with a coefficient of friction as $\mu=0.7$ and a shear friction factor as $m=0.9$. A sliding contact with a constant friction coefficient as $\mu=0.2$ is considered to represent the contact between the chip and the workpiece [18].

4 Comparison of predicted cutting forces

The predicted forces from FE models were compared to an empirical model developed from micro-end milling by utilizing cutting force measurements for Ti-6Al-4V alloy [15], where the tangential and radial cutting coefficients (K_t, K_r) can be obtained from the cutting speed v_c (m/min) and feed per tooth f_z (mm/tooth) as:

$$K_t = 2689\left(\frac{v_c}{v_{co}}\right)^{-0.239}\left(\frac{f_z}{f_{zo}}\right)^{-0.349}. \tag{2}$$

$$K_r = 2044\left(\frac{v_c}{v_{co}}\right)^{-0.133}\left(\frac{f_z}{f_{zo}}\right)^{-0.656}. \tag{3}$$

Due to the helicity of the micro-end mill, the contact region was distributed to n segments in the axial depth direction and the cutting forces in x and y direction can therefore be calculated by finding the summation of the forces in each segment as;

$$F_x(\phi) = \sum_{i=1}^{n} K_r \sin(\theta_i)A_{i,\phi} + K_t \cos(\theta_i)A_{i,\phi} \tag{4}$$

$$F_y(\phi) = \sum_{i=1}^{n} -K_r \cos(\theta_i)A_{i,\phi} + K_t \sin(\theta_i)A_{i,\phi} \tag{5}$$

where ϕ is the tool rotation angle measure at the tool leading edge, θ_i is the angle between element tool tip and the reference slide tool tip ($z=0$), and A_i is the uncut chip area at each segment.

$$A_{i,\phi} = \frac{a_p}{n}\left(f_z \sin(\theta_i) + R - \sqrt{R^2 - \left(f_z cos(\theta_i)\right)^2}\right) \tag{6}$$

$$\theta_i = \phi - (i-1)\frac{a_p \tan(\beta)}{R\,n} \tag{7}$$

The comparison given in Fig. 2 for the predicted cutting forces that is obtained by comparing forces from FEM simulations against the forces calculated from the empirical model based on micro-milling experiments given in [15] indicates good agreements validating the FE simulations for micro-end milling.

5 Predicted chip flow and burr formation

3-D chip flow together with local field variables such as temperature, elastic/plastic strain, strain-rate, and velocity in the shear zones are predicted using the FE models. The measurement methodologies of the shear angles, chip thickness and width, and top burr height and width are explained in Fig. 3.

The shear angles (ϕ_s) at different depths were measured between the cutting speed direction and lines of shear planes (Fig. 3a). The chip thickness (t_{chip}) and width (w_{chip})

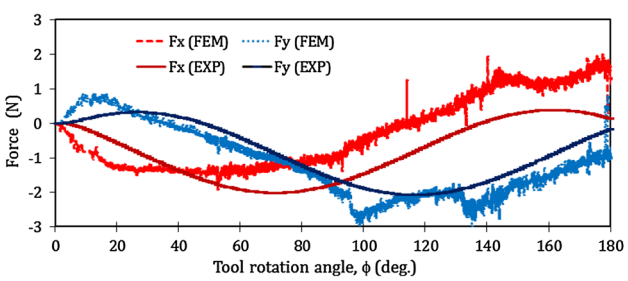

Fig. 2 Comparison of predicted forces with the empirical model

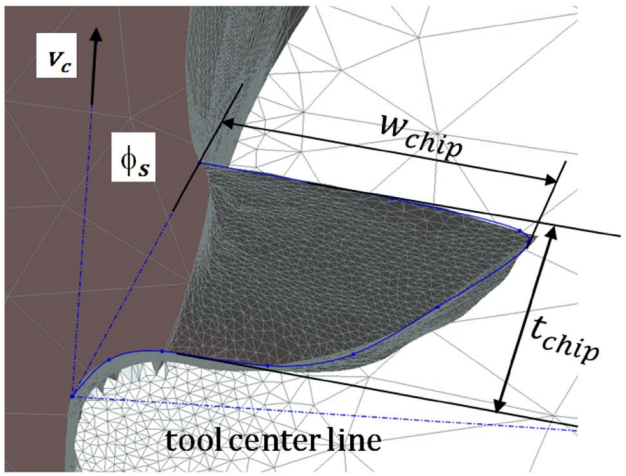

(a) Chip measurement.

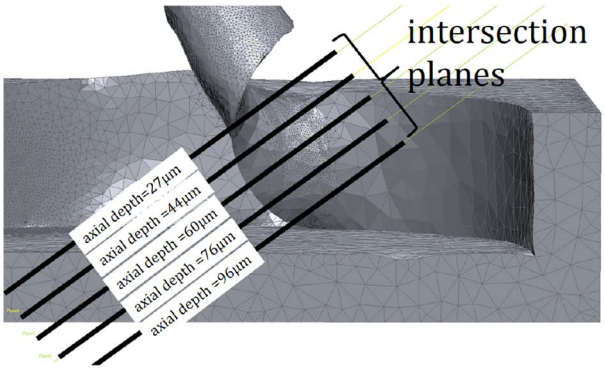

(b) Planes of intersection.

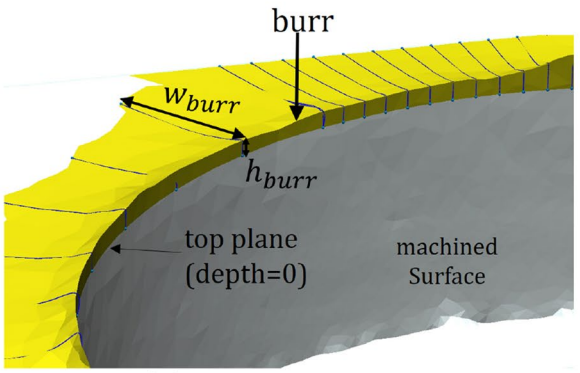

(c) Burr measurement.

Fig. 3 Measurement of shear angle, chip dimensions, and burr dimensions as obtained from FE simulation results

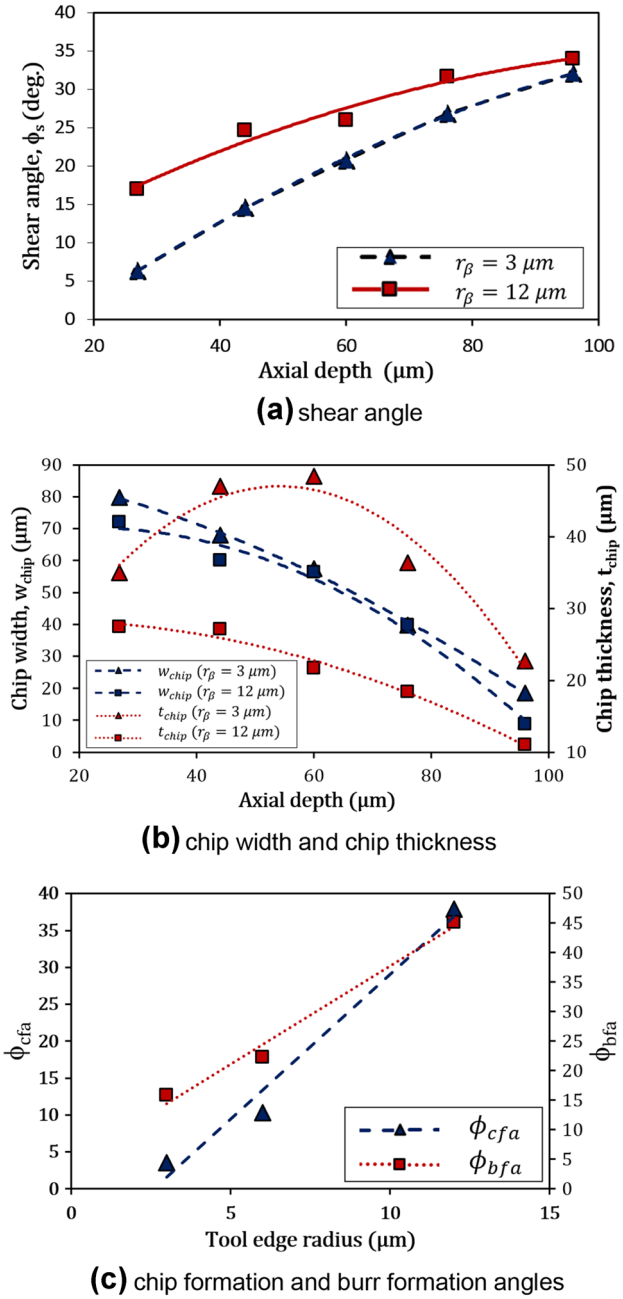

(a) shear angle

(b) chip width and chip thickness

(c) chip formation and burr formation angles

Fig. 4 Measured shear angle (**a**), chip width and thickness (**b**), and chip and burr formation angles, **c** in full immersion micro-end milling as obtained from the FE simulation results

were measured from extracting dimensions of intersection of mesh and planes shown in Fig. 3b. The height of top burrs formed on workpiece top surface (h_{burr}) was measured at different tool rotation angles (Fig. 3c). The results of normal shear angles, chip thickness and width, and the chip and burr formation angles after cutting using two edge radii are shown in Fig. 4.

The predicted shear angles are lower where the tool with small edge radius (unworn tool) is used. The chip was thicker when using the larger edge radius (worn tool). The burr formation angle was measured by evaluating the damage occurred on workpiece top surface, where the burr formation and chip formation angles behave similarly. Even though the damage value when using tool edge radius of $r_\beta = 3$ μm (unworn) was much lower than the damage value when using worn tools with edge radii of $r_\beta = 6$ μm and

Table 2 Comparison of predicted and measured average chip width and thickness with standard deviations

r_β (μm)	Predicted		Measured	
	w_{chip} (μm)	t_{chip} (μm)	w_{chip} (μm)	t_{chip} (μm)
3	105.3 ± 5.2	23.4 ± 2.5	113.7 ± 5.1	21.1 ± 1.9
6	112.2 ± 6.5	17.9 ± 2.0	88.9 ± 8.7	17.9 ± 3.5
12	101.8 ± 3.7	20.7 ± 0.6	111.7 ± 4.6	10.6 ± 0.8

$r_\beta = 12$ μm, the damage occurred after $\phi = 15.8°$ of the tool rotation and $\phi = 12°$ after the chip started to form. As summarized in Table 2, the results of chip width and chip thickness obtained from FE simulations can find acceptable agreement with the SEM images shown in Fig. 5. It should be noted that the measurement of chip width and chip thickness were taken at 180° tool rotation angle. The chip morphology as observed with SEM imaging indicates slight chip serration due to localized instability and ductile fracture. That behaviour is more dominant in macro scale milling of titanium alloys [17].

Figure 6 shows the equivalent plastic strain predicted for the three cutting tool edge roundness values representing unworn and worn cases. It is obvious that when using worn tools or tools having large edge roundness, high plastic strains remain on the workpiece machined surface resulting in high residual stresses.

6 Built-up edge formation

In machining titanium alloys due to intense adhesion of chip material creates a built-up along the tool cutting edge [12, 14]. The intensity of chip material on the tool cutting edge can be explained with stress distribution along the cutting edge of the micro end mill. Therefore, built-up edge (BUE) was identified by the sudden rise in stresses on tool edge. Figure 7 shows a close-up view of the worn tool edge indicating BUE formation and chip adhesion due to high stresses around the BUE region and the tip of the micro-end mill. In this figure worn section of the tool edge geometry and chip adhesion with built-up edge can be clearly observed. On the other hand, Fig. 8 shows the maximum principal stresses at the chip in front of the tool cutting edge starting from the workpiece top surface to its bottom machined surface. Typically, at the location along the tool cutting edge where workpiece surface (or at the zero depth of cut) is reached, the maximum principle stress is near zero but the compressive stress increases along the tool cutting edge with increase in the depth of cut direction and reaches to a peak compressive principle stress around a location where chip adhesion and BUE are observed.

The predicted results indicate that the height of BUE is smaller for a smaller edge radius (unworn with an edge

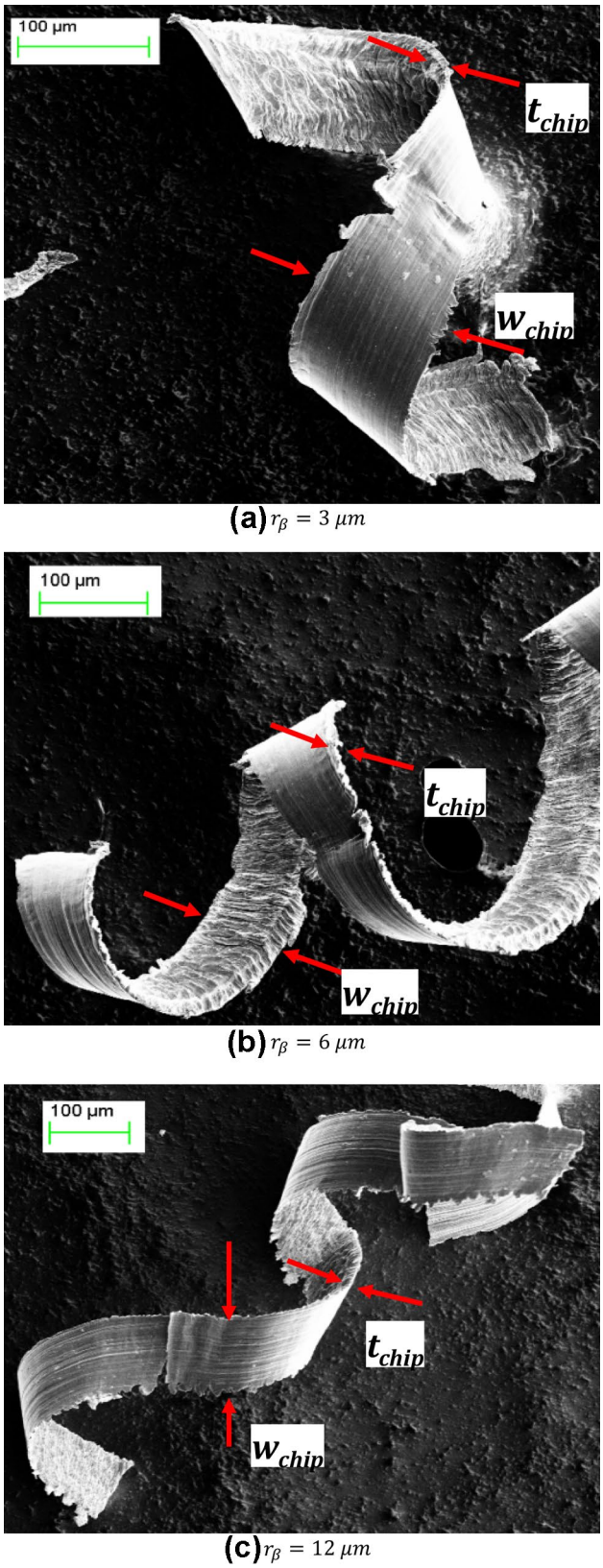

Fig. 5 SEM images of chip morphology obtained from micro-milling with increasing edge roundness due to worn tool edge geometry

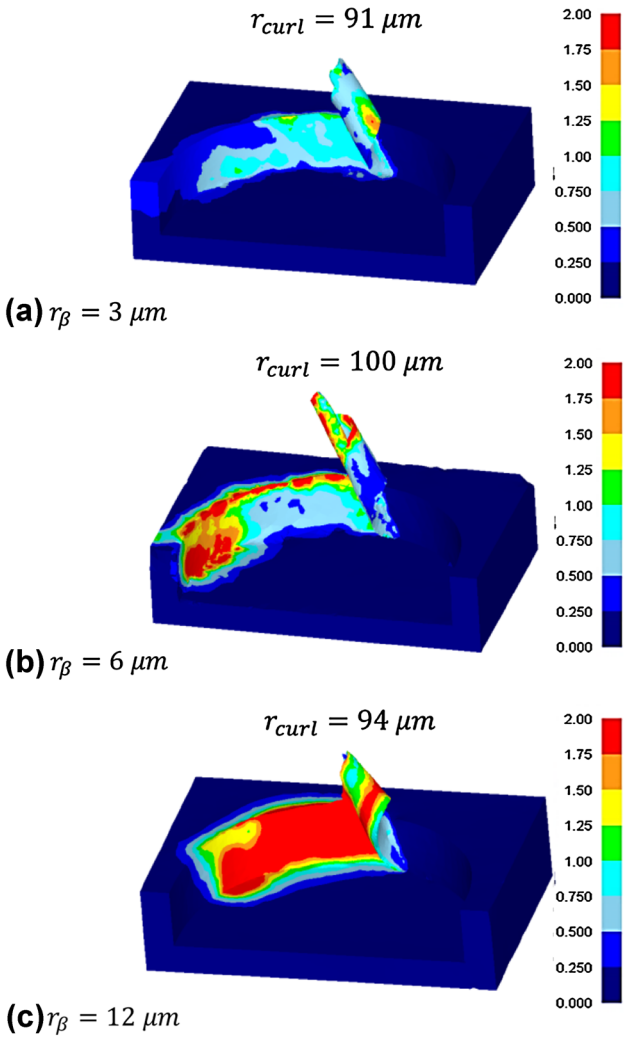

Fig. 6 Predicted equivalent plastic strain contours and chip flow with curl radius during full immersion micro-milling

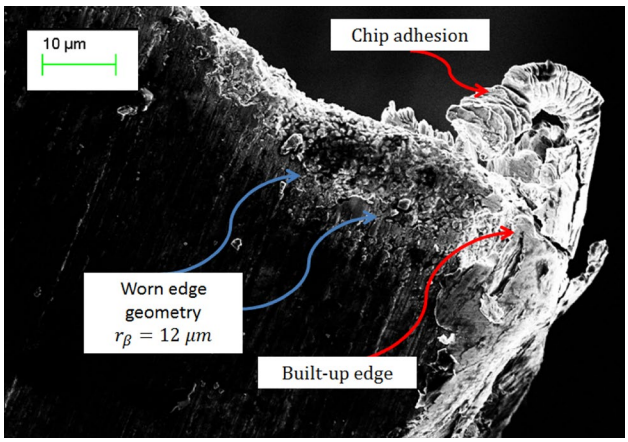

Fig. 7 SEM images of worn tool edge showing BUE formation

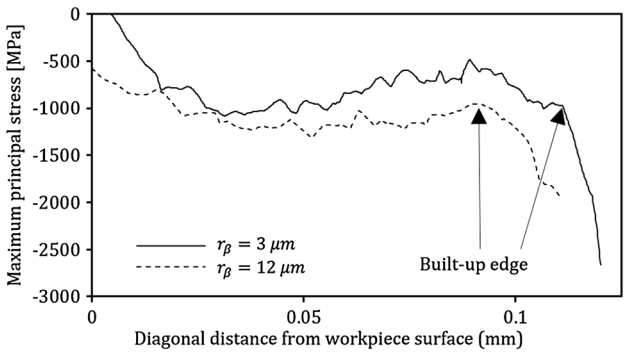

Fig. 8 Stress distribution on the cutting edge and at the BUE

roundness of $r_\beta = 3$ µm) tool than using a larger edge roundness tool ($r_\beta = 12$ µm) with significant tool wear. This stress distribution observation finds a good agreement with the SEM images, obtained for the micro-end mill tool after cutting a distance of $l_{cut} = 500$ mm in the cutting experiments.

7 Burr prediction model

Among the work on predicting burr height by using analytical modeling, the approach proposed by Ko and Dornfeld [10], where it is assumed that the all work that should be done for chip formation is going to be equal to generate burr formation, Eq. (8), was often used to calculate the entrance side burrs or exit side burrs [2]. Top burr formation can also be predicted by using an analytical approach following the works of Gillespie and Blotter [8] and Kruy et al. [11]. However, the current approach proposed in this paper is to use FE simulations along with burr analytical models since the analytical force prediction models are not accurate for worn tools especially when having tools with different edge radii or different tool edge geometry.

The formulation begins with calculating the work done for chip formation and burr formation by utilizing the predicted cutting forces from FE simulations for unworn and worn cutting tools and calculating the torque generated per tool rotation as given below;

$$W_{chip} = W_{burr} \tag{8}$$

$$W_{chip} = \sum_{\phi_{burr}}^{180} T(\phi)\Delta\phi \tag{9}$$

$$W_{burr} = \sum_{\phi_{burr}}^{180} \sigma_0\, a_p\, l_\phi \left[\frac{1}{\sqrt{3}} \left(l_\phi \cos\left(\beta_\phi\right) - l_{\phi+\Delta\phi} \cos\left(\beta_{\phi+\Delta\phi}\right) \right) + \left(l_\phi \sin\left(\beta_\phi\right) - l_{\phi+\Delta\phi} \sin\left(\beta_{\phi+\Delta\phi}\right) \right) \right] \tag{10}$$

where T, the torque at tool rotation angle ϕ, is obtained from FE simulations, ϕ_{burr} is the entrance side burr initiation angle, β_i and l_i are the instantaneous negative shear plane angle and length, respectively, and σ_0 is the yield stress. The entrance burr initiated after tool rotation of $\phi = 163°$ and $\phi = 168°$ for tool edge radii of $r_\beta = 3$ µm and $r_\beta = 12$ µm, respectively. The top burr formed during micro-milling could be predicted analytically. The same approach is used to predict the top burr, where the height and the width of top burrs can be calculated as [11],

$$h_{burr} = \frac{a_p(1+\nu)e^{-3\phi_a}}{\sqrt{3}E}\left[-\frac{\sin\phi_S}{2\sqrt{3}\cos\phi_S + 2\sin\phi_S}\right] \tag{11}$$

$$w_{burr} = r_\beta \left[e^{-3\phi_a}\sqrt{cos\phi_a} - 1\right] \tag{12}$$

where ν is Poisson's ratio, E is the Young's modulus, ϕ_s is the shear angle, r_β is the effective edge radius, ϕ_a is the plasticity ellipse angle, which can be calculated as,

$$\phi_a = -\sin^{-1}\left(\frac{\sqrt{3}P_o}{2\sigma_p}\right) + \frac{\pi}{6} \tag{13}$$

where P_o is the pressure on the tool edge, and σ_p is the plastic stress. These parameters (P_o, σ_p, ϕ_s) are taken from the FE simulations and the predicted results on top burr heights and widths are given in Table 3.

FE simulation results are used in measuring burr heights. Figure 9 shows the average top burr height resulted from three tools (unworn, slightly worn, and worn) with different edge radii during up (beginning) and down (ending) milling sections of full immersion milling. It is obvious that tool edge roundness contributes to the top burr formation since a larger edge radius of worn tool resulted in larger top burrs. The top burr therefore is more likely to form when the tool edge radius is larger or worn.

The top burr formation in full immersion micro milling has been observed in micro milling of titanium alloy Ti-6Al-4V under the same cutting conditions described in experimental section for micro milling of concentric circular slots. Field emission SEM images of the top burrs indicate around $h_{burr} = 5$–15 µm top burr heights using unworn tool with an approximate edge roundness of $r_\beta = 3$ µm, whereas the worn tool with an approximate edge roundness of $r_\beta = 12$ µm resulted in top burr heights larger than $h_{burr} = 10$ µm as they are given in Table 3 and shown in Fig. 10. This indicates that some improvements to predict top burr formation by using analytical modelling approach as an extension to FE simulations can be formulated with proper adjustments to be adopted for micro milling processing conditions.

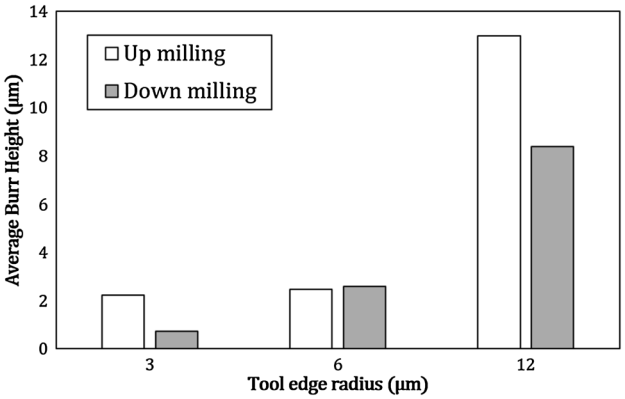

Fig. 9 Effect of increasing tool edge roundness on the burr height during up and down milling section of full immersion micro-end milling as measured from FE simulation results

8 Conclusions

This study presents experimental and simulation based investigations on the effect of increasing tool edge roundness due to tool wear on the formation of 3-D chip flow, top burrs, chip adhesion and BUE formation in micro-end milling by using 3-D FE simulations. Predicted forces are compared against the experimental models indicating good agreements and validating FE simulation predictions. These models were further used to investigate the effect of increasing tool edge roundness due to tool wear on the chip and burr formation angles and the influence of the milling strategy (up milling and down milling) on the top burr height. The results show reasonably good agreement between FE simulations and experiments in terms of predicting forces, chip flow, and chip dimensions. In addition, an extension to implement an analytical top burr prediction model using FE simulation results is presented. Some specific conclusion can be given as:

Table 3 Burr model parameters together with a comparison of predicted and measured results

r_β (µm)	P_o (MPa)	σ_p (MPa)	ϕ_S (mean)	Predicted burrs		Measured burrs	
				h_{burr} (µm)	w_{burr} (µm)	h_{burr} (µm)	w_{burr} (µm)
3	2430	2700	20	1.9	10	5–15	20–50
12	2250	2700	26	5.1	46	10–30	50–150

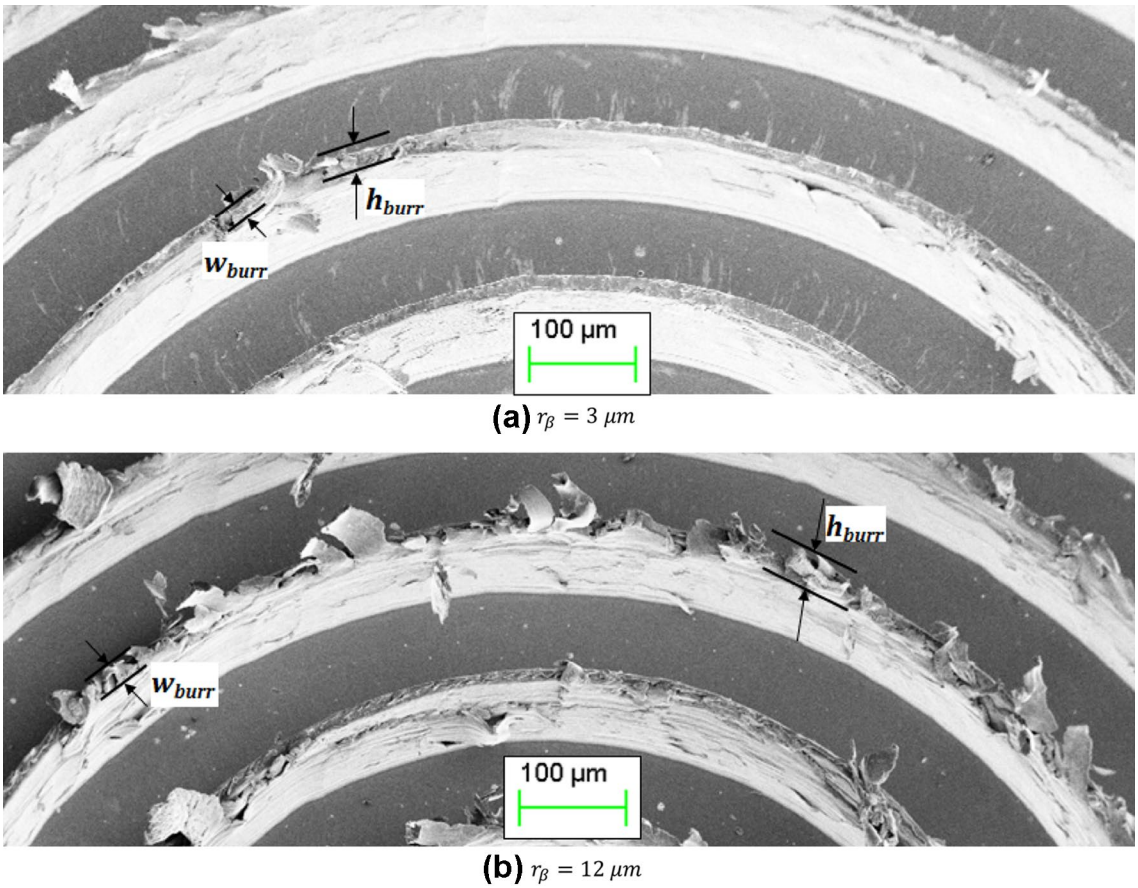

Fig. 10 Top burr formation during full immersion micro-milling of titanium alloy Ti-6Al-4V; **a** unworn tool and **b** worn tool

- 3-D FE simulations using work material constitutive model for predicting cutting forces is reasonably acceptable.
- 3-D chip flow with associated plastic strain, shear angles, chip formation and burr formation angles can be predicted.
- Shear angle increases with increasing axial depth of cut and further increase with increasing cutting edge roundness.
- Chip formation takes place at a much higher tool rotation angle due to increase in tool edge roundness and associated ploughing effect.
- BUE can be explained by monitoring the stress distribution along the chip-tool contact, since the maximum principle stress at tool surface location is correlated with the chip adhesion and built-up edge formation.
- Top burrs, burr height and width dimensions, and chip curling increase with an increasing tool edge roundness due to tool wear which can be predicted fairly accurately by using an analytical model.

Acknowledgements The support provided by DEFORM software by SFTC, Ohio, USA is gratefully acknowledged.

References

1. Altintas Y, Jin X (2011) Mechanics of micro-milling with round edge tools. CIRP Ann Manuf Technol 60(1):77–80
2. Aurich JC, Dornfeld D, Arrazola PJ, Franke V, Leitz L, Min S (2009) Burrs—analysis, control and removal. CIRP Ann Manuf Technol 58:519–542
3. Biermann D, Kahnis P (2010) Analysis and simulation of size effects in micromilling. Prod Eng Res Dev 4(1):25–34
4. Chen MJ, Ni HB, Wang ZJ, Jiang Y (2012) Research on the modeling of burr formation process in micro-ball end milling operation on Ti-6Al-4 V. Int J Adv Manuf Technol 62:901–912
5. Denkena B, Biermann D (2014) Cutting edge geometries. CIRP Ann Manuf Technol 63:631–653
6. Dornfeld D, Mina S, Takeuchi Y (2006) Recent advances in mechanical micromachining. CIRP Ann Manuf Technol 55:745–768
7. Gelfi M, Attanasio A, Ceretti E, Garbellini A, Pola A (2015) Micromilling of lamellar Ti6Al4V: cutting force analysis. Mater Manuf Process 31(7):919–925

8. Gillespie LK, Blotter PT (1976) The formation and properties of machining burrs. Trans ASME Ser B 98(1):66–74
9. Jaffery SI, Mativenga PT (2009) Assessment of the machinability of Ti-6Al-4V alloy using the wear map approach. Int J Adv Manuf Technol 40:687–696
10. Ko SL, Dornfeld DA (1996) Analysis of fracture in burr formation at the exit stage of metal cutting. J Mater Process Technol 58(2–3):189–200. doi:10.1016/0924-0136(95)02124-8
11. Kruy S, Aoyama H, Ohta K, Sano N (2014) Prediction of thickness and height of burr based on burr formation mechanisms in end milling. Bull JSME 8(4):14-00084
22. Özel T, Thepsonthi T, Ulutan D, Kaftanoğlu B (2011) Experiments and finite element simulations on micro-milling of Ti-6Al-4V alloy with uncoated and cBN coated micro-tools. CIRP Ann Manuf Technol 60(1):85–88
12. Oliaei SNB, Karpat Y (2016) Investigating the influence of built-up edge on forces and surface roughness in micro scale orthogonal machining of titanium alloy Ti6Al4V. J Mater Process Technol 235:28–40
13. Özel T, Bartolo P, Ceretti E, Ciurana J, Rodriguez CA, Lopes Da Silva JV (2016) Biomedical devices: design, prototyping and manufacturing. Wiley, Hoboken
14. Pramanik A, Littlefair G (2015) Machining of titanium alloy (Ti-6Al-4V)—theory to application. Mach Sci Technol Int J 19:1–49
15. Riviere-Lorphevre E, Letot C, Ducobu F, Dehombreux P, Filippi E (2017) Dynamic simulation of milling operations with small diameter milling cutters: effect of material heterogeneity on the cutting force model. Meccanica 52:35–44
16. Schulze V, Autenrieth H, Deuchert M, Weule H (2010) Investigation of surface near residual stress states after micro-cutting by finite element simulation. CIRP Ann Manuf Technol 59:117–120
17. Storchak M, Jiang L, Xu L, Li X (2016) Finite element modeling for cutting process of the titanium alloy Ti10V2Fe3Al. Prod Eng Res Dev 10(405):509–517
18. Thepsonthi T, Özel T (2015) 3-D finite element process simulation of micro-end milling Ti-6Al-4V titanium alloy: experimental validations on chip flow and tool wear. J Mater Process Technol 221:128–145
19. Thepsonthi T, Özel T (2016) Simulation of serrated chip formation in micro-milling of titanium alloy Ti-6Al-4V using 2D elasto-viscoplastic finite element modeling. Prod Eng Res Dev 10(6):575–586
20. Uhlmann E, Oberschmidt D, Kuche Y, Löwenstein A (2014) Cutting edge preparation of micro milling tools. Proced CIRP 14:349–354
21. Wang JJ, Uhlmann E, Oberschmidt D, Sung CF, Perfilov I (2016) Critical depth of cut and asymptotic spindle speed for chatter in micro milling with process damping. CIRP Ann Manuf Technol 65(1):113–116